EARTH SURFACE PROCESSES AND LANDFORMS
Earth Surf. Process. Landforms **34**, 1878–1893 (2009)

Published online in Wiley InterScience
(www.interscience.wiley.com) DOI: 10.1002/esp.1872

Effects of Holocene climate and sea-level changes on coastal gully evolution: insights from numerical modelling

Julian Leyland* and Stephen E Darby
School of Geography, University of Southampton, Highfield, Southampton, UK

Received 16 June 2008; Revised 11 December 2008; Accepted 9 June 2009

*Correspondence to: Julian Leyland, School of Geography, University of Southampton, Highfield, Southampton, SO17 1BJ, UK. E-mail: J.Leyland@soton.ac.uk

ESPL
Earth Surface Processes and Landforms

ABSTRACT: Gullies are sensitive to a range of environmental disturbances so they can provide insight into the environmental history of surrounding landscapes. Coastal gullies are of particular interest as they are influenced by terrestrial and marine processes. For example, the coastal gullies found on the Isle of Wight, UK, are highly dynamic, with episodes of sea cliff erosion causing rejuvenation of the channel network. Consequently a key factor in their long-term evolution is the relative balance between rates of cliff retreat (driven primarily by Holocene sea-level rise) and headwards incision caused by knickpoint migration (driven primarily by Holocene climate via its impact on runoff). In this paper we explore the Holocene erosional history of these gullies using a numerical landscape evolution model modified to include a cliff recession function. Knickpoint recession rates are simulated using a detachment-limited erosion law wherein erosion rate is a power function of drainage area and stream gradient with model parameters defined using empirically-derived data. Hindcast simulations, from 12 000 cal. years BP to present, are undertaken for a range of scenarios of Holocene climate change and sea-level rise. Plausible erosional histories are extracted from scenarios in which simulated and observed gully forms match. The results suggest that rate of sea-level rise is the key control on gully formation and that it is only in the late Holocene period, and specifically in the last 2000 years, that sea-level rise has slowed sufficiently for knickpoint recession rates to exceed cliff recession rates and create sustainable gully networks. The simulations also indicate that the contemporary gully systems are close to a critical threshold, suggesting that future gully evolution is likely to be sensitive to small changes in rates of effective precipitation and/or sea-level rise. Copyright © 2009 John Wiley & Sons, Ltd.

KEYWORDS: Holocene; sea-level change; climate change; gully erosion; knickpoint; landscape evolution

Introduction

Gullies form when runoff accumulates in narrow channels and removes the underlying material of the channel to considerable depths (Poesen *et al.*, 2003). They are found in various shapes and sizes in all regions of the world, and although they are often initially ephemeral in nature, it is well documented that they can become a permanent part of the drainage system (Poesen *et al.*, 2003; Boardman and Poesen, 2006). Gully formation processes are similar to those found operating in incised river channels, and both are associated with high volumes of sediment output. Indeed, the sediment output from a network of gullies or incised channels often represents much of the sediment yield from that landscape (Schumm *et al.*, 1984; Simon *et al.*, 1996; Valentin *et al.*, 2005). The derived sediment may be stored in bars, floodplains and terraces and therefore has a significant impact on downstream morphology and ecology. Additional impacts on in-stream ecology result from increased suspended sediments and mobile streambeds, which affect water quality and spawning habitats (Greig *et al.*, 2005; Suren *et al.*, 2005).

In addition to their practical significance, investigations of gully dynamics have revealed that gullies are sensitive to a wide range of environmental disturbances (Stankoviansky, 2003; Vanwalleghem *et al.*, 2003, 2005; Ambers *et al.*, 2006; Chiverrell *et al.*, 2007). These studies indicate that the geomorphology of gully systems may provide a proxy record of the environmental history of the surrounding landscape. As such, attempts have been made to model the relationship between environmental change and gully initiation and evolution (Vandekerckhove *et al.*, 2000; Nachtergaele *et al.*, 2001). These investigations follow the approach adopted in a number of studies that have attempted to replicate morphologies of existing geomorphological features using landscape evolution models (LEMs). In such studies, hindcast simulations that replicate observed contemporary morphologies are deemed to

offer some insight into the formative processes and associated environmental conditions (Howard, 1997, 1999; Coulthard, 1999; Coulthard *et al.*, 2000, 2002; Istanbulluoglu *et al.*, 2005).

At the land adjacent to both oceans and lakes, where cliffs or bluffs are found, there is the potential for the formation of a specific type of gully. When stream channels have the excess energy required to cut down through the cliff to reach the outlet water body, an 'incised coastal channel' (Leyland and Darby, 2008) can form. Sea cliffs are ubiquitous, occurring along ~80% of the Earth's ocean coasts, with similar features bordering lakes and other large water bodies (Emery and Kuhn, 1982), and their associated gullies must therefore also be widespread. However, few detailed assessments of incised coastal gully processes and evolution have been carried out (Schumm and Phillips, 1986; Burkard and Kostaschuk, 1995; Hampton and Griggs, 2004; Bishop *et al.*, 2005). This is surprising because these features are of special interest in that they are strongly influenced by both terrestrial and marine processes. As such, investigations of the erosional histories of these features, in a manner analogous to the studies introduced earlier, may afford insights into marine and terrestrial environmental change.

This research focuses on a particular set of incised coastal channels (known locally as 'Chines') that debouche (up to 45 m) the soft cliffs of the southwest coast of the Isle of Wight, southern England (Figure 1). Although the southwest coast of the island is relatively sparsely populated, the Chines are nationally recognized both as a special area of conservation (SAC) and a site of special scientific interest (SSSI). The Chines offer a combination of an extension of the soft cliff resource as well as more sheltered locations up stream. In conjunction with the bare substrate (a requirement of many invertebrate species), which is maintained through mass-wasting processes, they provide habitat for plant (*Philonotis marchica*, *Anthoceros punctatos*) and invertebrate (*Psen atratinus*, *Baris analis*, *Melitaea cinxia*) species of international importance.

The base level of the Chines is highly dynamic, with episodes of sea cliff erosion causing the rejuvenation of the channel network. Consequently a key factor identified in Chine evolution is the relative balance between rates of cliff retreat (governed by sea-level rise) and headwards incision caused by knickpoint migration (Leyland and Darby, 2008). Specifically, if contemporary coastal retreat rates are higher than the corresponding rates of knickpoint recession, there is a long-term reduction in the overall extent of the Chines and their associated habitats. In this paper we explore the Holocene 'erosional history' (*sensu* Howard, 1997, 1999) of the Chines using a numerical LEM [the Geomorphic/Orogenic Landscape Evolution Model (GOLEM); Tucker and Slingerland, 1994, 1997]. The model is parameterized to represent a series of scenarios that explore whether (i) the contemporary channels are relic (i.e. no longer actively incising) components of a prior channel system that has now been truncated by coastal erosion

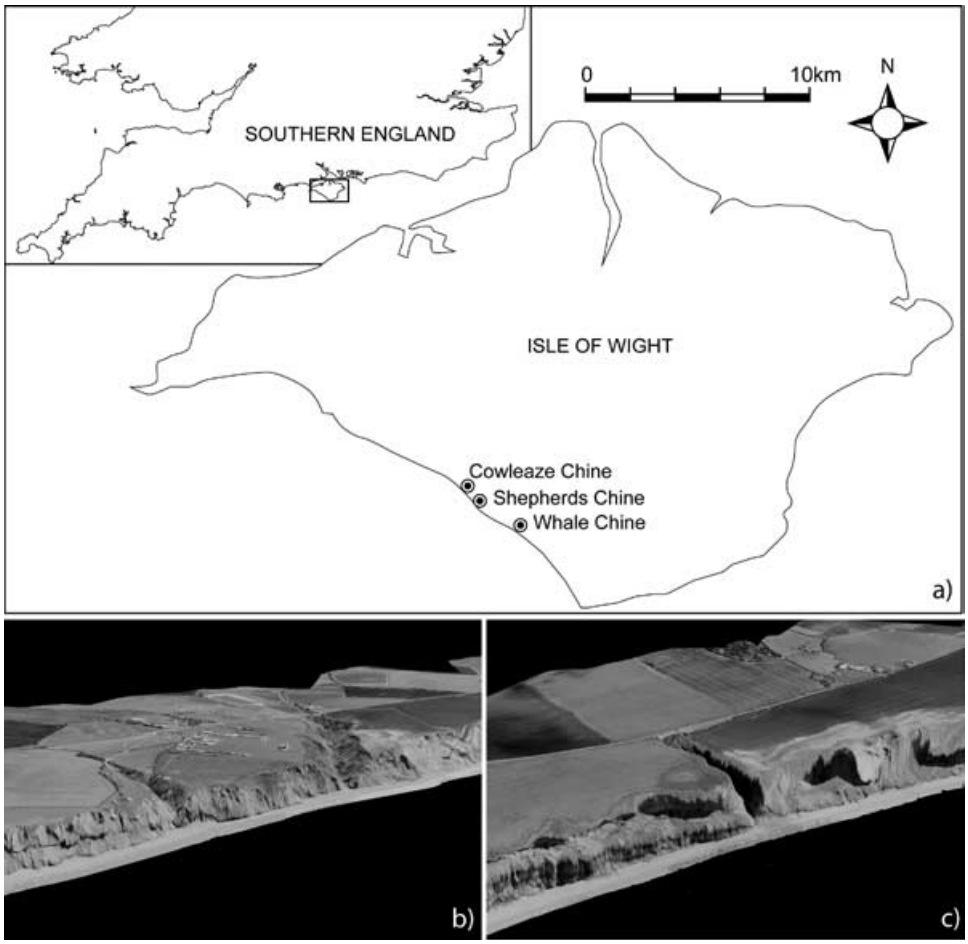

Figure 1. (a) Location of the Isle of Wight and the named gullies (known locally as 'Chines') along the southwest coast. Aerial photographs of (b) Cowleaze Chine (left) and Shepherds Chine (right) and (c) Whale Chine draped over 2 m resolution Lidar digital elevation data (data courtesy of the Channel Coastal Observatory). Cowleaze Chine is in a state of decay, as evidenced by the abrupt step where the gully meets the shore, whereas Shepherds and Whale Chines are in a stable state (downstream extents reach equilibrium with sea-level). See Leyland and Darby (2008) for further details.

DOI: 10.1002/esp

during Holocene sea-level rise, or (ii) whether the channels are actively incising in response to base-level changes forced by shoreline cliff retreat. In the case of the former scenario, ancillary questions relate to the extent to which the incision was associated with low sea-level stands or climatic shifts, and in the latter case the range of contemporary rates that form plausible Chine features. Each scenario forms the basis for a hindcast simulation extending across the Holocene (12 000 BP to present) with 'plausible' erosional histories being identified as those scenarios for which the model outputs at the end of the hindcast match contemporary Chine morphologies. To our knowledge no prior study has employed numerical LEMs in this way to establish the relationship between environmental drivers (climate, sea-level change and cliff retreat) and gully evolution in the specific context of coastal gullies.

Study Site Description

Regional setting

The Isle of Wight is located off the central southern English coast and is part of a major geological structure called the Hampshire Basin. The geology of the island is varied, being divided by a central east-west ridge formed in a vertically dipping stratum of Upper Chalk. The geology to the north of the ridge is dominated by Oligocene sands, clays and shales which are divided by small rivers which drain north into the Solent (Bird, 1997). South of the ridge lies a truncated anticlinal basin consisting mainly of Lower Greensand formations. At the southernmost tip of the island the land rises again to a cap of Chalk with a ledge of Gault clay found at the base of the outcrop. The Chines of the southwest coast are found cut through the Gault Clay, Lower Greensand and Wealden Beds along the southwest coast (Daley and Insole, 1984).

Of principal importance to the erosional history of the Chines is the progression of sea-level changes during the Holocene. These have been studied comprehensively for the British Isles as a whole (Lambeck, 1991; Clark and Mix, 2002; Shennan and Horton, 2002) and also locally (Nicholls, 1987; Long and Tooley, 1995; Velegrakis *et al.*, 1999, 2000; Edwards, 2001). The rising sea-levels of the mid to late Holocene re-occupied former despoiled cliffs re-initiating erosion of the soft Cretaceous sands and clays to form a rapidly retreating linear or slightly embayed cliff coastline. These actions have left behind a shallow near-shore shelf stretching some 4 km into the English Channel and it is thought that this delimits the magnitude of the late Holocene coastal recession (Bray *et al.*, 2004). The coastal retreat has been limited in certain localities by the occurrence of more resistant strata forming the northwest and southeast extremities of the coastal section.

During glacial periods, when the sea level was very low, a substantial easterly flowing river, the Solent, drained the Hampshire Basin (West, 1980; Barber, 1987; Nicholls, 1987; Tubbs, 1999). The basin was limited to the south by the Wight-Purbeck ridge, a chalk ridge that joined the two areas, the remnants of which are evident today in the chalk stacks known as The Needles. The course of the Solent River is important as it explains many geological deposits of fluvial origin and it is likely that input tributaries, such as the western arm of the River Yar, would have been far more extensive (Figure 2). Pleistocene deposits suggest that a river may have run somewhere along or south of, the present southwest coast of the Isle of Wight. However, the eroding coastline has truncated the Western Yar, suggesting that much of the land lost to erosion was part of the drainage basin of this river. It is therefore unclear whether the Chines are relic features, originally formed as part of this larger palaeo-system, or whether they are more recent, active, features.

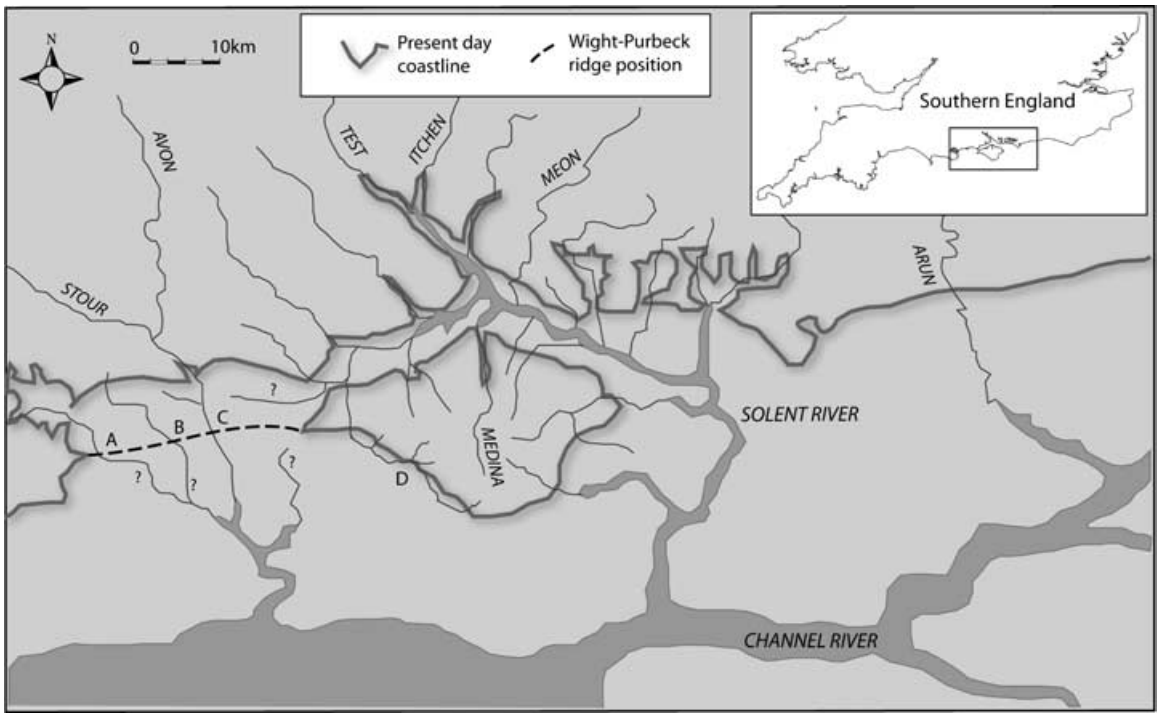

Figure 2. Location of the Isle of Wight and estimated shoreline and flow path of the Solent River at *c.* 12 000 BP. A, B and C mark the locations of possible breaches of the Wight-Purbeck ridge. D marks the possible route of the extended Western Yar river. Adapted from Bray *et al.* (2004) after Velegrakis *et al.* (1999, 2000).

DOI: 10.1002/esp

Methods

Model overview

The GOLEM developed by Tucker and Slingerland (1994, 1996, 1997) is well suited for use in this research. GOLEM operates by solving a mass balance equation across an orthogonal grid of square cells. The processes of uplift and erosion that influence the components of this balance are in turn simulated by a set of process equations (Figure 3). Full details are reported in Tucker and Slingerland (1997) and are not repeated here, but a summary is instead provided in the Appendix.

Although GOLEM has successfully been employed in a wide range of applications (Tucker and Slingerland, 1994, 1996, 1997; Tucker and Bras, 1998; Tucker and Whipple, 2002), like other LEMs it does not account for any coastal processes. For the purposes of this study, where we are interested in accounting for the effects of climate change through the Holocene, the original version of GOLEM is further limited in that its input data files cannot be used to specify an arbitrarily varying climate. We have therefore modified GOLEM by including two new modules, created in a MATLAB (Mathworks, 2008) programming environment, that are used to update (i) the elevations in the grid cells along the lower boundary of the model (to account for coastal recession associated with sea-level rise) and (ii) the main input file (to adjust the climate) during each iteration of a model run. As indicated in Figure 4, implementation of these process modules initially involves running GOLEM for a short period (e.g. 50 years) using a user defined digital elevation model (DEM) and input file. The output files from this short simulation are then time-stamped and stored for later analysis. The update functions are then run; in the case of sea-level rise and cliff retreat this involves manipulation of the DEM, whereas to alter the climate the input file is simply re-written. Once the updated DEM and the new input file are created, GOLEM is re-run for another short period, the process being repeated until the total model run time is reached.

The effects of sea-level as a dynamic base level and the associated cliff retreat, which creates knickpoints at the mouths of the Chines, have been proposed by Leyland and Darby (2008) as being key aspects of Chine creation and maintenance. As mentioned earlier, these marine processes are not currently included in any of the published LEMs, and as such additional process function modules were developed. Both the rate of sea-level rise in the Solent region (Everard, 1954; Nicholls, 1987; Velegrakis *et al.*, 1999, 2000; Nowell, 2000) and the relationship between the rate of cliff retreat forced by rising sea-levels (Bray and Hooke, 1997; Lee, 1997; Lee and Clark, 2002; Walkden and Dickson, 2006) have received considerable attention, with contemporary cliff retreat rates also available (Leyland and Darby, 2008). That there is a link between sea-level rise and cliff retreat is well established (Bray and Hooke, 1997), but while data exist to parameterize sea-level rise through the Holocene period (see

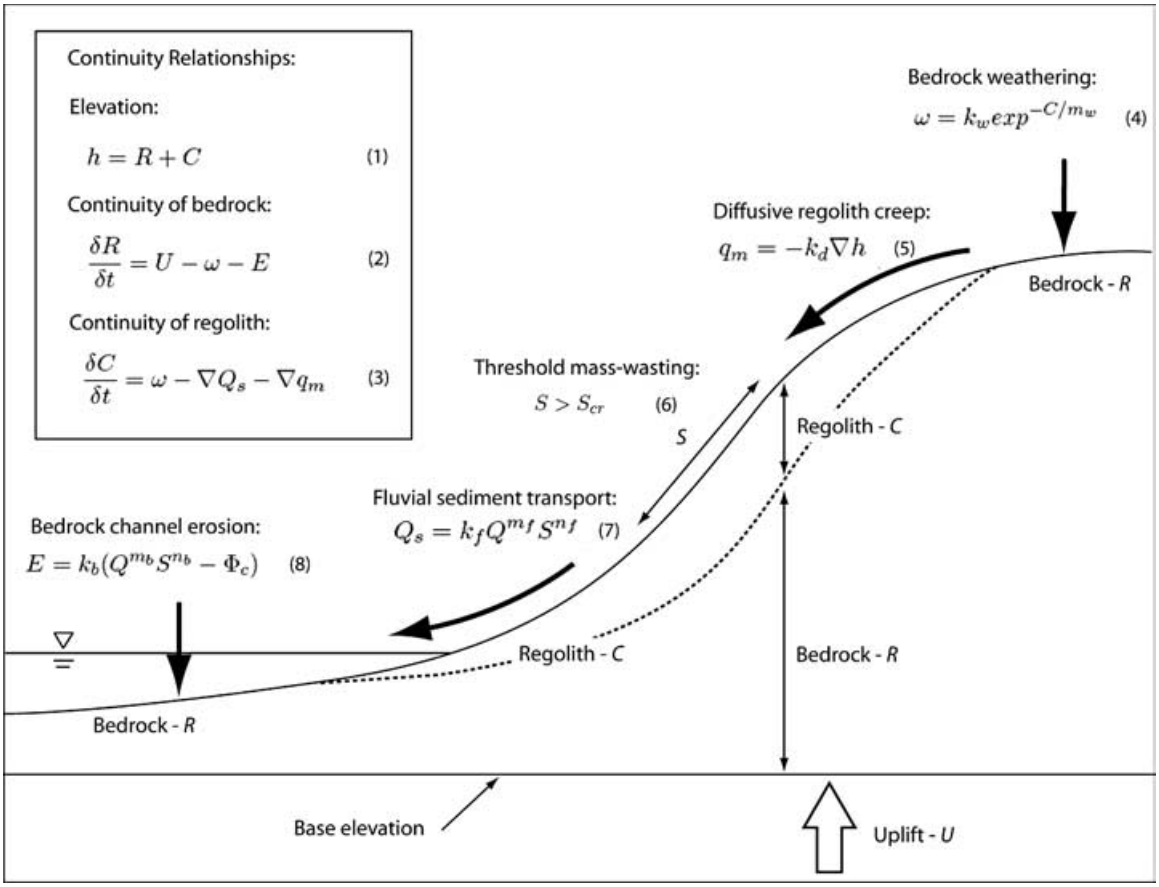

Figure 3. Representation of the key relationships and geomorphic processes in GOLEM (after Tucker and Slingerland, 1997). Definition of symbols: h, elevation of cell; R, bedrock depth; C, regolith depth; t, time; U, rate of uplift; ω, weathering rate; E, rate of bedrock channel erosion; Q_s, rate of fluvial sediment transport; q_m, volumetric rate of hillslope mass movement; Q, discharge; S, slope; S_{cr}, critical slope for mass-wasting; k_b, bedrock erodibility coefficient; m_b, discharge exponent for bedrock erosion; n_b, slope exponent for bedrock erosion; Φ_c, threshold for bedrock erosion; k_f, fluvial sediment transport coefficient; m, fluvial transport discharge exponent; n, fluvial transport slope exponent; k_d, diffusivity coefficient; k_w, bare bedrock weathering rate coefficient; m_w, decay depth constant.

DOI: 10.1002/esp

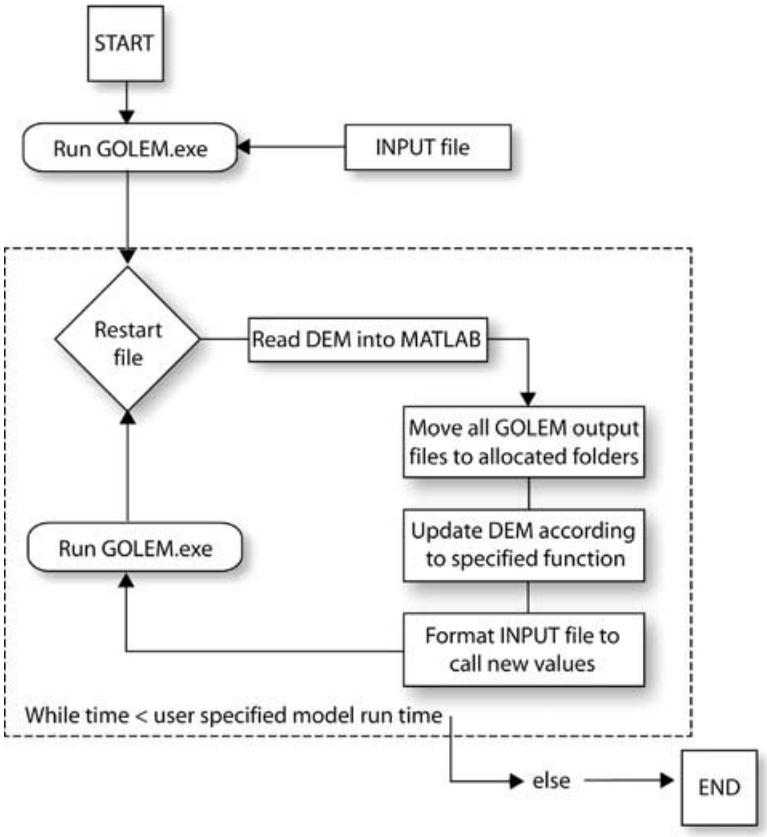

Figure 4. Flow chart representation of the modelling process, showing how the custom process functions are implemented.

the section entitled 'Base case scenario'), associated data for the shoreline cliff position are limited. Despite this there are some forms of evidence such as the shallow marine shelf that extends some 4 km, and which is thought to mark the late Holocene cliff retreat (Bray *et al.*, 2004), and there are estimates of pre-Holocene shore positions (e.g. Velegrakis *et al.*, 1999, 2000; Bray *et al.*, 2004). These data can be combined and regressed ($R^2 = 0{\cdot}99$, $n = 4$, $p > 0{\cdot}05$) to give a non-linear relationship between cliff-retreat rate (CRR) and sea-level rise (SLR) of the form:

$$\mathrm{CRR} = 22{\cdot}4\mathrm{SLR}^{0{\cdot}5} \quad (1)$$

In comparison to the cliff recession and SLR update scripts the climate change function is very straightforward. In between sub-runs a value for effective precipitation (the variable used to characterize climate, this being a reasonable proxy of mean annual runoff) for the defined run time is simply read in from an ASCII text file.

Model parameterization

It is clear from Figure 3 that GOLEM's process sub-models include a large number (12, see Table I) of adjustable parameters, so careful consideration must be given to the selection of their values. Note that these parameter values remain constant in all the simulations, such that the simulation scenarios differ only in the values of the driving variables (climate and sea-level change) used therein (see section entitled 'Model scenarios').

The Chines are predominantly bedrock features, and as such, fluvial transport of regolith material is not considered a key process. Nonetheless if realistic landscapes are to be modelled it is important to include a fluvial function as this governs the initiation and spatial extension of the channel network prior to the onset of bedrock erosion processes (Leopold *et al.*, 1964; Summerfield, 1991; Knighton, 1998). In this study a fluvial transport function based on a simple generic power law function (Equation A7 in the Ap[pendix and Figure 3) was used, with the slope (n_f) and area (m_f) exponents set to 0·4 and 1, respectively, identical to the values of the bedrock erosion parameters derived later. The parameter k_f governs the efficiency of the transport, and this was set to a value of one, meaning that initial fluvial erosion of the upper regolith will be highly efficient (Tucker and Slingerland, 1997).

The bedrock erodibility coefficient, k_b, and the area exponent, m_b, have previously been derived empirically for both the Shales and Marls and the Lower Greensand lithologies, with full details provided in Leyland and Darby (2008). The slope exponent, n_b, was here set at a value of one for consistency with the 'stream power' law relationship (Tucker and Whipple, 2002). The slope exponent (n_b) is in fact known to depend on the dominant erosion process, Whipple *et al.* (2000) arguing that its value varies between ~2/3 and ~5/3. Tucker and Whipple (2002) note that the behaviour of LEMs varies critically with the choice of n_b, finding that $n_b = 1$ induces parallel retreat of stream profiles, consistent with our observations that Chine knickpoints maintain marked steps as they migrate upstream (Leyland and Darby, 2008).

The critical shear stress of the bedrock in which the Chines are cut (Equation A8 in the Appendix, and on Figure 3) was measured directly using a cohesive strength meter (CSM) according to the methodology of Tolhurst *et al.* (1999). The Chines are found in two key geologies; the Wealden Shales and Marls and the Lower Greensand beds. In view of this, field

DOI: 10.1002/esp

Table I. Summary of values and method of derivation for the parameters used in the simulations

Parameter	Units	Value	Method/source of derivation
k_f, fluvial sediment transport efficiency	–	1	Set at 1 to enable maximum sediment transport efficiency (Tucker and Slingerland, 1997)
m_f, fluvial sediment transport slope exponent	–	0·4	Set at same value as bedrock erosion exponent (see below)
n_f, fluvial sediment transport area exponent	–	1	Set at same value as bedrock erosion exponent (see below)
k_b, bedrock erodibility	$m^{0·2}$ a^{-1}	0·015	Area-slope modelling – see Leyland and Darby (2008) for full details
m_b, bedrock erosion area exponent	–	0·4	Area-slope modelling – see Leyland and Darby (2008) for full details
n_b, bedrock erosion slope exponent	–	1	Set at 1 to induce parallel knickpoint retreat – see Leyland and Darby (2008) for details
F_c, bedrock erosion threshold term	N m^{-2}	3·6	Direct measurement using *in situ* cohesive strength meter (n = 11)
k_w, bedrock sediment production rate	m a^{-1}	0·0005	Set according to those values used by Tucker and Slingerland (1997) for the WE-38 temperate catchment in Pennsylvania, USA
m_w, sediment production decay depth	m	0·5	As above
k_d, hillslope diffusivity coefficient	m^2 a^{-1}	0·01	Values derived from Rosenbloom and Anderson (1994) and Tucker and Slingerland (1997) for a similar small, temperate catchment
S_{cr}, critical gradient for regolith landslides	m m^{-1}	4	Set at very high value (76°) to effectively 'switch off' regolith landsliding
S_{cr}, critical gradient for bedrock landslides	m m^{-1}	0·7	Direct measurement of Chine banks· $Tan^{-1}(0·7) = 35°$, which is the upper limit of slopes observed in the field – see Leyland and Darby (2008) for full details

tests were carried out in Shepherds Chine and Whale Chine which incise through these two types of bedrock. The critical shear stress for the Shales and Marls is double that of the Lower Greensand lithology (Shepherds Chine) at 3·6 ± 1·3 N m^{-2} (n = 11; error estimates correspond to one standard deviation) compared to the value of 1·8 ± 0·3 N m^{-2} (n = 5) measured at Whale Chine. As most of the Chines are found in the Shales and Marls the value derived for this geological unit is used in the simulations.

There has been relatively little work on long-term rates of bedrock denudation that might be useful in parameterizing the weathering coefficients (k_w) and exponents (C, m_w) (Equation A4 in the Appendix and on Figure 3), although in the context of this study it is not considered to be of high importance due to the time scale (last 12 000 years) of interest. The studies that have been undertaken make use of dated structures (e.g. grave stones or buildings) or the newly emerging fields of low-temperature thermochronology (e.g. Kohn *et al.*, 2002) or the analysis of *in situ* terrestrial cosmogenic nuclides (e.g. von Blanckenburg *et al.*, 2004). Bishop (2007) cites characteristic long-term rates of denudation for tectonically stable, non-glaciated settings as varying between 0·000005 and 0·00001 m a^{-1}, although these rates are acknowledged as being low. When parameterizing GOLEM for simulations of the WE-38 watershed, a 7·2 km^2 temperate catchment in Pennnsylvania, USA, Tucker and Slingerland (1997) set k_w to a value of 0·0005 m a^{-1}. This catchment is probably more representative of a typical Chine catchment in that it is small, has erodible geologies of sandstone and shales and receives approximately 1 m a^{-1} of rainfall, similar to the value of approximately 0·7 m a^{-1} for the Isle of Wight. Tucker and Slingerland (1997) set the sediment production decay constant (m_w) at 0·5 m, a relatively large depth, probably indicative of the relatively high erodibility of the catchment. Mottershead (1997) cites denudation rates of sandstone as high as 0·0038 m a^{-1}, although these were calculated over a short (38 years) time period. Average rates over a 105 year period are lower at 0·0006 m a^{-1}. These rates are similar to those used by Tucker and Slingerland (1997), and as such they are used for this study (see Table I), although it is important to note that uncertainty analysis of ±100% error in these terms yielded no significant changes in landscape output over 12 000 years, confirming the insignificant impact of the choice of these parameters on the results presented herein.

The Isle of Wight Chine catchments are small, low relief drainage basins and are not affected by threshold colluvial land sliding; as such the threshold slope for landslide initiation is set at a sufficiently high value (4 m m^{-1}) to effectively remove this process from consideration. The catchments are likely to be affected by slow diffusive processes and the hill-slope diffusivity coefficient, k_d, is set at 0·01 m^2 a^{-1} following the studies of Rosenbloom and Anderson (1994) and Tucker and Slingerland (1997). The critical gradient for bedrock sliding (which GOLEM can model), S_{cr}, is estimated using the morphological information developed in Leyland and Darby (2008), which allows the minimum angle for sliding to be constrained. In combination with calibration runs which assessed the impact of the grid domain and cell size upon the Chine bank simulation outputs, the parameter is set at a value of 0·7 m m^{-1}, the equivalent of a critical bank slope angle of 35° (Table I).

Model scenarios

To assess what combinations of Holocene environmental change have resulted in the creation and maintenance of the Chines, simulation scenarios were constructed to represent a plausible range of variation in the key driving variables of effective precipitation and SLR (Table II). The parameterized models for these scenarios can be regarded as a set of multiple working hypotheses of environmental changes that may have affected Chine evolution. A hypothesis is falsified if the corresponding hindcast simulation fails to accurately replicate the contemporary morphologies, as discussed later. The model scenarios were initially designed around a base case that represents our best estimate of the actual variations of climate and SLR through the Holocene. Additional scenarios were then developed to explore a variable range of environmental changes around the base case so as to (i) account for the effects of any uncertainty in the base case scenario and to (ii) explore additional scenarios that might be helpful in identifying the specific conditions under which the Chines have formed.

Base case scenario: Holocene climate and sea-level changes
Equation 1 indicates that the successful simulation of Holocene cliff retreat, which in turn provides the basic forcing (via the

DOI: 10.1002/esp

Table II. Scenarios employed in the numerical simulations of Chine evolution

Scenario	Description	ΔP (× base rate)	ΔSLR/CRR (× base rate)
1	Base case (best estimate – see text) conditions	1	1
2	Wetter climate and increased rates of sea-level rise and cliff retreat	1·5	1·25
3	Drier climate and decrease in sea-level rise and cliff retreat	0·5	0·75
4	Wetter climate with decrease in sea-level and cliff retreat	1·5	0·75
5	Wetter climate with base case sea-level and cliff retreat	1·5	1
6	Drier climate and increased sea-level and cliff retreat	0·5	1·25
7	Drier climate and base case sea-level rise and cliff retreat	0·5	1
8	Base case climate and rapid sea-level rise and cliff retreat	1	1·25
9	Base case climate and decreased sea-level rise and cliff retreat	1	0·75
10	Contemporary climate and sea-level rise and cliff retreat throughout duration of the run	Set at 0·4 m a^{-1} for run	SLR set at 0·002 m a^{-1}, CRR set at 0·5 m a^{-1}

Note: ΔP is the change in effective precipitation, ΔSLR is the change in sea-level rise, the latter controlling the cliff retreat rate, CRR, via Equation 1.

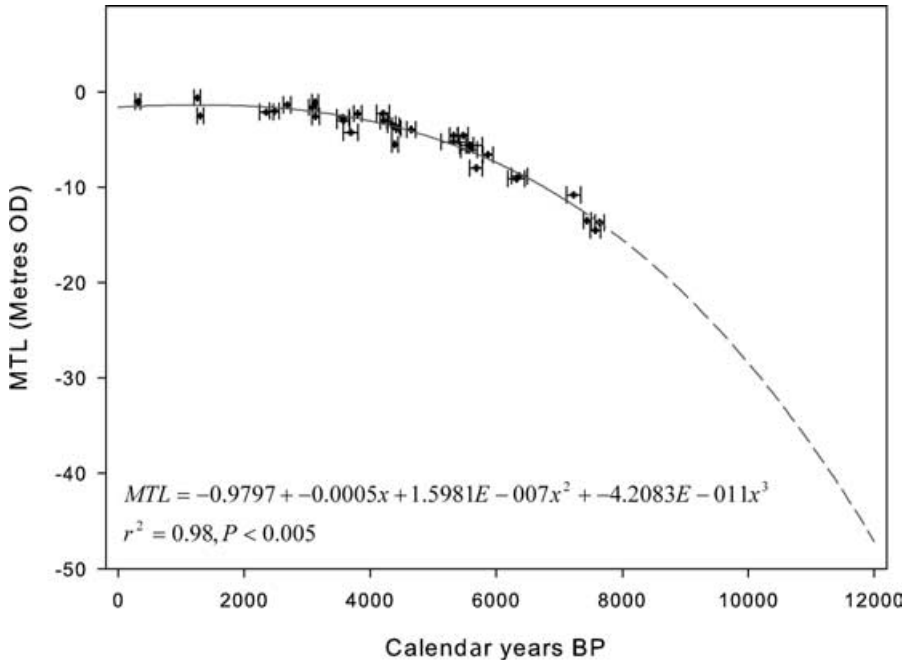

Figure 5. Relative sea-level changes in the Solent region regressed using a cubic polynomial function to allow the estimation of sea-levels at dates for which there is no data (dashed line). The estimated sea-level of approximately –45 m at 12 000 BP is consistent with estimates in the literature (e.g. Dyer, 1975; Tubbs, 1999). The error bars represent the overall dating error comprising the statistical counting uncertainty and the calibration error surrounding the calendar dates. MTL = mean tide level. Data assimilated from Long and Tooley (1995) and Long *et al.* (1999, 2000) by Waller and Long (2003) with additional data from Edwards (2001).

cliff retreat rate) for changes in base-level throughout the model simulations, is dependent upon a robust set of dated sea-level altitudes in the region. Data has been assembled from various studies (Long and Tooley, 1995; Velegrakis *et al.*, 1999; Edwards, 2001; Shennan and Horton, 2002) and regressed using a cubic polynomial function (R^2 = 0·98, p > 0·005, n = 35) to allow the derivation of an empirical sea-level curve for the Solent region (Figure 5). Sea-levels prior to 8000 cal. years BP are projected using the regression equation earlier, which predicts a sea-level of approximately –45 m at 12 000 cal. years BP, consistent with the broad range of estimates ranging from –46 m at 14 000 cal. years BP from Dyer (1975) to –35 m at 11 000 cal. years BP from Tubbs (1999).

While reliable data to define Holocene SLR are available, unfortunately many UK terrestrial studies of palaeo-climate use proxy data from peat cores or speleothems, so there are very few data sources specifically for southern England. Indeed, a comprehensive search revealed that there are no complete Holocene climate reconstructions for this location. It was, therefore, necessary to utilize data from further afield, similar to the manner in which Coulthard *et al.* (2002) used the northern Scottish record of Anderson *et al.* (1998) in a modelling study of a small upland catchment in North Yorkshire, UK. It should also be noted that many of the more complete palaeo-climate proxies are based on temperature driven records, including the bog surface wetness record used by Couthard *et al.* (Barber and Langdon, 2001). Nevertheless, such records still offer some insight into the general nature of past climates, assuming that in temperate climatic regions warm periods are accompanied by an increasing trend of effective precipitation and cool periods vice versa (Langdon, personal communication, 2008). In view of this, and in light of the lack of alternative records, the most suitable proxy record appears to be the area-averaged time series reconstructions of mean annual surface air temperatures for Europe developed by Davis *et al.* (2003). The data set covers the last 12 000 years, and is based on quantitative pollen climate reconstructions from over 500 pollen sites that have been

DOI: 10.1002/esp

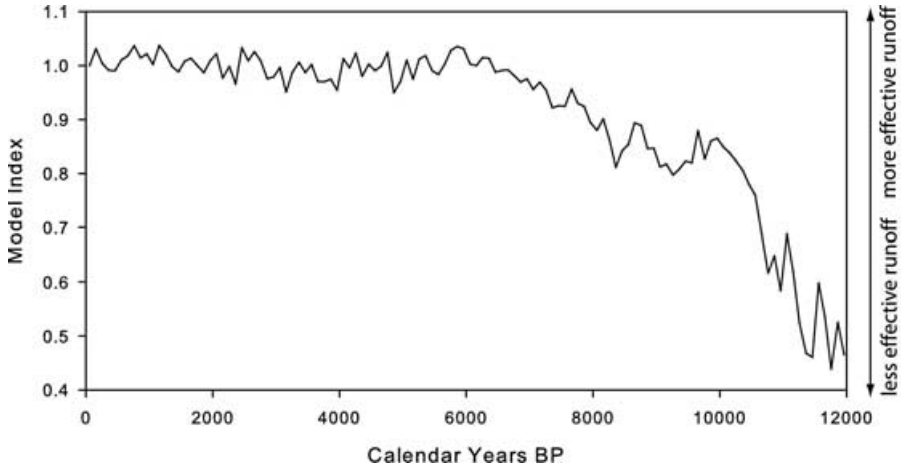

Figure 6. Climate data of Davis *et al*. (2003) for central western Europe represented as a normalized model index where one represents the estimated contemporary (1961–1990) effective precipitation of 0·4 m a^{-1}.

assimilated onto a four-dimensional grid of 1° squares at a temporal resolution of 100 years. The grid data was subsequently amalgamated into six larger areas covering Europe, and climatic data extracted from each of the six areas. We used the data from the central western region as this contained our area of interest. We then modified the time series by normalizing the temperature anomaly to create a model factor (Figure 6), where 1 represents contemporary climatic conditions. In GOLEM climate is represented by effective precipitation (i.e. the difference between rainfall and evaporation), so the value of 1 in the model index was then finally equated to a current rate of effective precipitation. For the 1961–1990 period this was estimated to be ~0·4 m a^{-1} based on the outputs of Arnell's (2003) global runoff model, the latter being parameterized using the New *et al*. (1999) global climatology at 0·5° resolution.

Other scenarios

The remaining scenarios outlined in Table II were designed to explore the range of possible rates of driving condition changes (specified here using the change in effective precipitation, ΔP, and the change in sea-level rise, ΔSLR, the latter controlling the cliff retreat rate, CRR, via Equation 1) that may or may not result in realistic incised coastal gully formation. These scenarios were derived by simply multiplying the base case rates by the factors shown in Table II, with the exception of Scenario 10, where contemporary driving condition rates were used throughout the duration of the model run.

Model initialization and boundary conditions

One issue with undertaking hindcast simulations is the obvious difficulty of precisely estimating the correct initial conditions (specifically, it is necessary to specify the initial elevations for each cell in the computational grid) for a point in the distant past (12 000 BP here). In light of the uncertainties inherent in reconstructing a precise pre-historic DEM our simulations rely on the use of an analogue DEM that is intended to represent the essential attributes of the terrain at 12 000 BP. This was constructed by retaining an overall catchment morphology based on the contemporary terrain and assuming, based on the information summarized in Figure 2, that the pre-Holocene shoreline extends a distance of some 14 km south of the existing one. This was achieved using the maximum Chine catchment elevation as a starting point and fitting a randomly perturbed power function surface through a point representing the contemporaray shore position, extending to a point at approximately −45 m below current sea-level 14 km further south. This initial DEM was then used as the basis for a 'spin-up' simulation of 5000 years duration in which CRR = 0 m a^{-1}. The output DEM from the 'spin-up' was subsequently used to initialize all the model scenarios since it presents a more realistic drainage network and surface topography (Figure 7). Regarding the model boundary conditions, the bottom edge (looking at Figure 7) is dealt with by the update routine described earlier, and water and sediment are effectively removed as they flow across the boundary. The top boundary is closed and no water or sediment can exit across it, whilst the lateral boundaries of the model are open, periodic boundaries. That is, water and sediment that exit across a lateral boundary re-enters on the opposite side.

Results

Results from the simulations presented in Table II are initially detailed later (in the section entitled 'Description of results'), prior to discussing the comparisons between model predictions and observed metrics from the contemporary Chines in the section entitled 'Comparisons with contemporary Chine morphologies'.

Description of results

The general catchment characteristics for each scenario vary in a predictable manner that is determined primarily by the extent to which SLR has forced erosion of the shoreline back into the catchment hinterlands. The key element of interest is the presence (or lack) of gully features and their morphology at model time 12 000 years (T = 12 000). In view of this, Figure 8 provides close up, plan-view, images of part of the output model domains, focusing on the region at the cliff edge, and thus revealing the relative size of the gullies formed. In fact, gullies at T = 12 000 are evident in all but one of the models, that being Scenario 6 (see Table II for scenario descriptions), though there is considerable variation in the extent of simulated gully networks amongst the different model scenarios. For example, the output from the base case Scenario 1 shows that a relatively extensive gully feature has formed, stretching about 850 m inland. In this case, incision appears to have

DOI: 10.1002/esp

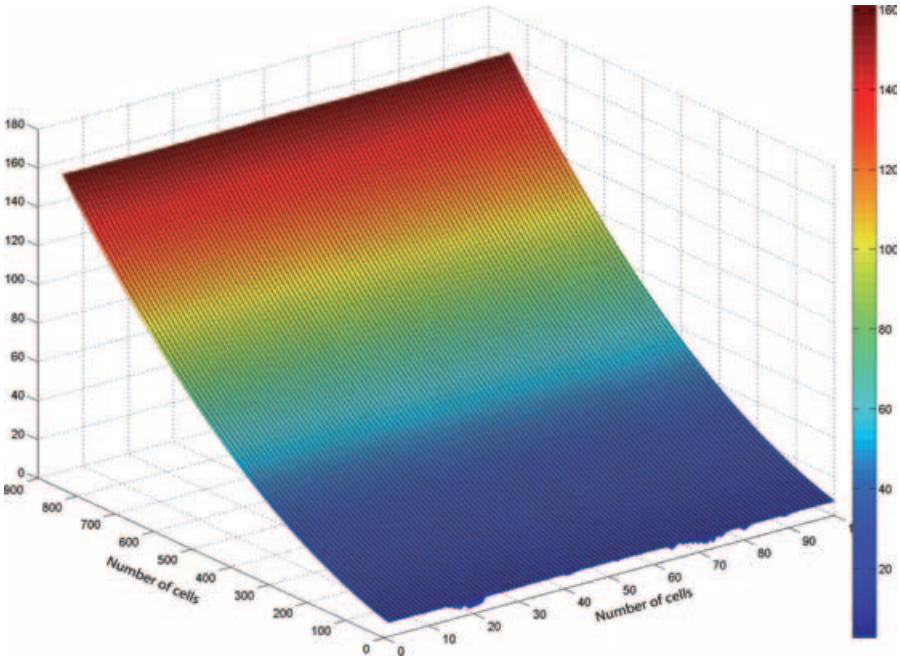

Figure 7. DEM representing an analogue of the landscape terrain at 12 000 BP. This DEM was reconstructed by extending the contemporary catchment slope to the estimated position of the shoreline at 12 000 BP and running a 5000 year GOLEM 'spin-up' simulation. This DEM is used as the initial condition in all subsequent simulations reported in this study. Note that the axes are not scaled, and that the DEM extends 22·5 km to the shore position, although it is only 2·5 km wide. This ensures realistic contemporary Chine catchment morphologies following a model run. Note also that the cell size is 25 m.

extended along an input tributary from the main stream. Scenarios 4, 5 and 9 also exhibit highly extensive gully networks (1300–1875 m), with main gullies that feature multiple headcuts and the presence of secondary gullies (marked on Figure 8) that are in some instances as far-reaching as the main features found in other scenarios. In contrast, the single gullies formed in Scenarios 7 and 8 are relatively short and narrow, reaching inland only ~200 m. Scenarios 2, 3 and 10 exhibit gullies that extend further inland (400–625 m) than in Scenarios 7 and 8, and which also have wider mouths at their downstream limits (ranging from 75 to 100 m in width, compared to approximately 25 m for Scenarios 7 and 8).

For reasons of clarity we do not offer details of how each of the simulated gully networks have evolved through time, rather we concentrate here on the base case Scenario 1 as an example of spatial and temporal development. Figure 9 shows model outputs from this scenario at T = 4000, 8000 and 12 000 years. Figure 9 indicates that by T = 4000 (Figure 9a) a cliffed shoreline (of about 10 m in height) has formed as the sea-level rise and associated shoreline recession begins to erode a step-like profile at the coast. As time progresses the cliff becomes more substantial in height (~20 m by T = 8000, Figure 9b), due to the rising trend of the land mass into which it is being cut. By the end of the model run the cliff is well developed, standing more than 30 m in height in places along the coast (Figure 9c).

Figures 9(d), 9(e) and 9(f) offer cross-section views through a small part of each of the cliff profiles described earlier. These plots reveal the rising sea-levels of the scenario, highlighting the timing of the formation of the gully that cuts through the cliff. Early in the simulation (T = 4000 years, Figure 9d) it appears that the cliff recession induced by rapidly rising sea-levels (see Figure 5) is large enough to prevent the establishment of a significant gully. However, by T = 8000 years (Figure 9e), the rate of erosion has diminished sufficiently to allow the formation of a fairly large gully (~15 m in depth at the coast) that, by the end of the model run (T = 12000 years, Figure 9f) is well developed. Indeed, by this time there appear to be some secondary incisions (e.g. at x = 1 and x = 3), albeit limited in extent to the very edge of the cliff profile.

Comparisons with contemporary Chine morphologies

To assess which model scenarios produce gullies which are most closely matched to contemporary Chine forms, a series of landscape and gully metrics were developed and used to compare modelled versus observed land forms. These metrics are broken down into two groups: general catchment metrics and gully metrics. The catchment metrics are used to compare the morphology of the drainage basins that feed the simulated gully networks and comprise (i) the mean catchment slope (S), calculated by averaging the local cell slope across the output DEM; (ii) the normalized hypsometric integral (HI); and (iii) the concavity index (θ). The concavity index is the ratio of the area and slope exponents (m_b/n_b) from Figure 3 and is estimated via regression analysis of local slopes log-binned by drainage area (Stock and Montgomery, 1999; Tucker and Whipple, 2002; Whipple and Tucker, 2002; Crosby and Whipple, 2006). The regression coefficients directly yield values for the exponent, m_b, and k_s, which is the normalized steepness index (Wobus *et al.*, 2006), as described earlier. Metrics used to characterize the forms of the gullies themselves include (i) the longitudinal slope, calculated as the slope of the gully from the mouth at the cliff to the headcut at the inland extent; (ii) width to depth ratio at the gully mouth; (iii) mean bank angle at the gully mouth; and (iv) the gully extent. In all cases observed values of the metrics have been quantified in the study by Leyland and Darby (2008).

The values of the simulated and observed metrics are compared in both Figure 10 and Table III. Figure 10 plots the ratios of modelled to observed metrics for each of the seven key comparative metrics across the 10 model scenarios. To

DOI: 10.1002/esp

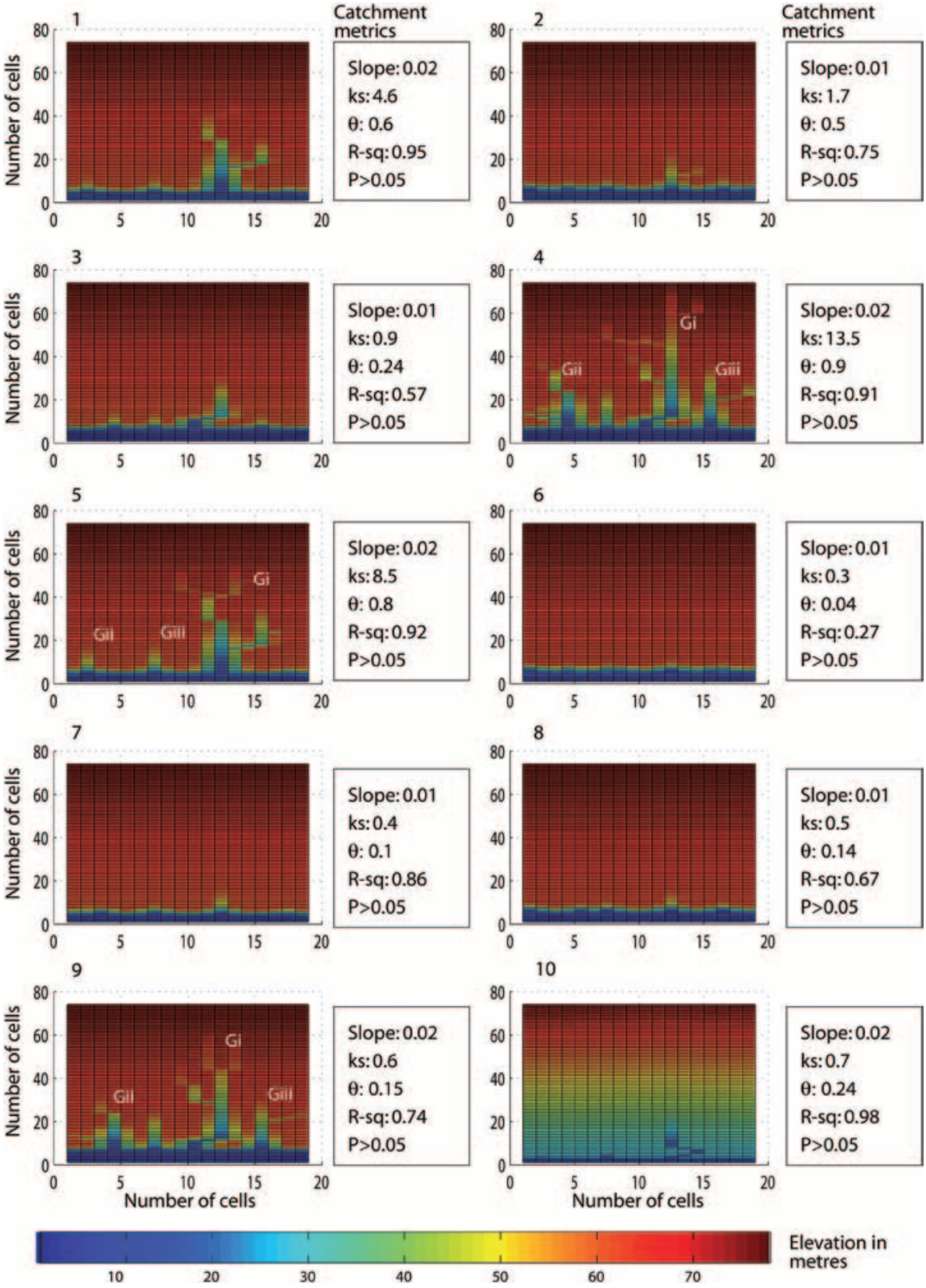

Figure 8. Model output at 12 000 years (i.e. at present day) showing close up of gully formation (where it occurs) for each of the scenarios presented in Table II (simulation number above the plot). Where multiple gullies exist, the label Gn refers to the corresponding metrics in Table III. The boxes to the right of each plot present the catchment metrics derived from the full model DEM output. Note that the cell size is 25 m, slope is given in units of m m^{-1} and the *p* value indicates the significance of the estimated coefficients at the 95% confidence interval. This figure is available in colour online at www.interscience.wiley.com/journal/espl

facilitate analysis of which model exhibits the optimal fit against the observed data, we aggregated the metrics by computing root mean square error (RMSE) values for each scenario and these are also illustrated (Figure 10). It is immediately clear that the characteristics of the modelled landscapes (as opposed to the gully forms themselves) differ from those of the contemporary catchments feeding the gullies (Figure 10d). Specifically the mean slope of all the modelled catchments is significantly less (by a factor of ~0·2–0·4) than that observed in reality (Figure 10a), just as the hypsometric integral is higher (by a factor of about ~2·0–2·2; Figure 10c). These errors are essentially artefacts of the DEM used to initialize the model

DOI: 10.1002/esp

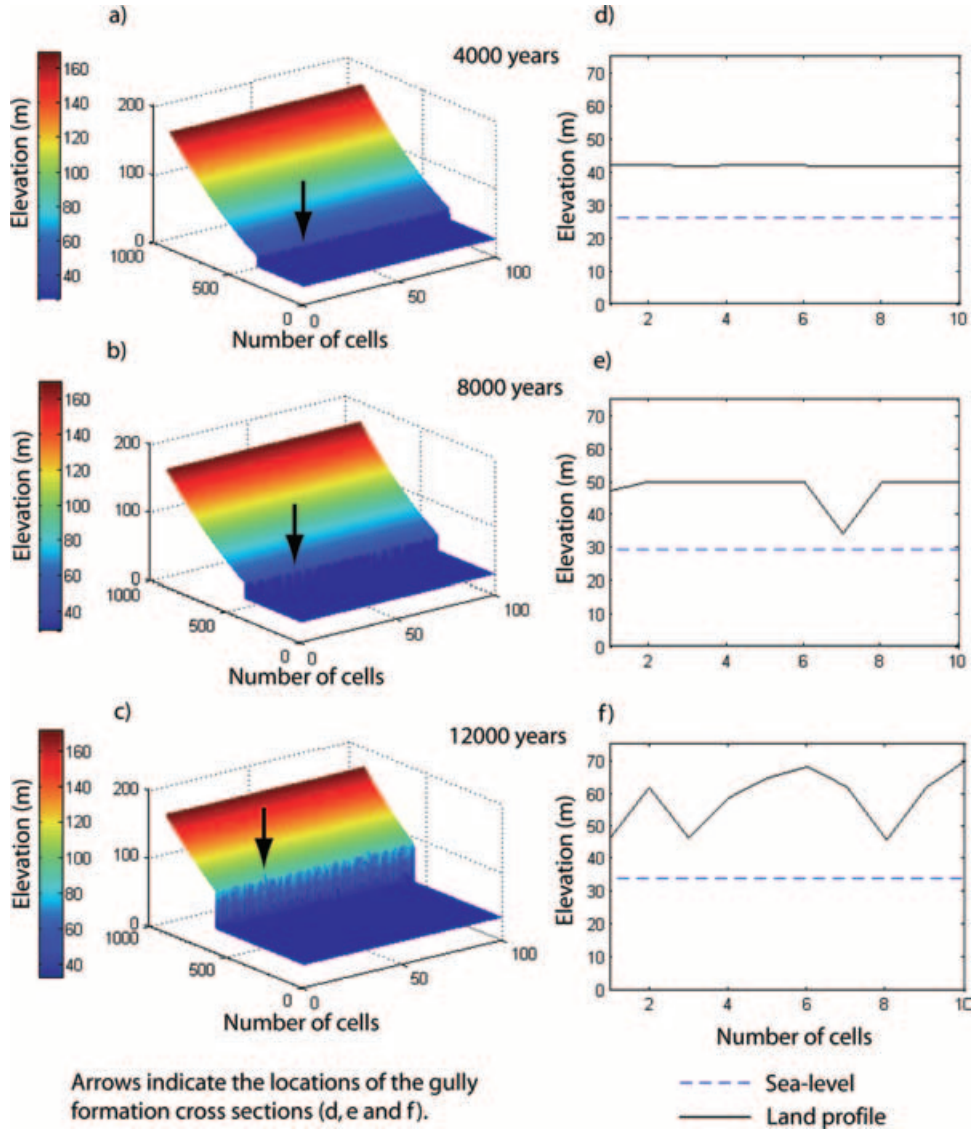

Figure 9. Model output for Scenario 1 (base estimate) at 4000, 8000 and 12 000 years. (a), (b) and (c) show the full outputs from the model, highlighting the sea-level rise and associated formation and retreat of the cliff profile. (d), (e) and (f) show a cross section of a portion of the cliff profile [indicated with arrows on (a), (b) and (c)], highlighting the development of coastal gullies through time.

runs. The high observed mean slope and low hypsometric integrals (Table III) of the contemporary catchments point to catchments which are well developed in terms of their drainage networks. Although the input DEM was subjected to a 'spin-up' simulation of 5000 years, it seems likely that this was insufficiently long to replicate a realistic landscape. The range of ratios of modelled/observed values for θ, the concavity index, does encompass those observed in the Chines on the Isle of Wight (Figure 10b). Scenario 2, in particular, is within a standard deviation of the observed value, but due to the issues just noted, too much credence should not be placed in this result (though see later).

In contrast, some of the simulated gullies do appear to match observed contemporary gully forms (Figure 10j). However, it is worth noting that our best estimate of Holocene rates of climate and sea-level change (Scenario 1), whilst showing a relatively good degree of fit between modelled and observed metrics, is not the optimal fit. The best overall fits based on the optimized fit for all available metrics (Figure 10e) are for Scenarios 2 (RMSE = 1·11), 7 (RMSE = 0·94) and 8 (RMSE = 0·98), primarily due to the more realistic gully extents simulated in these scenarios. In contrast, all of the other models result in very poor optimized fits (RMSE > 1·7), such that they can be discounted as plausible scenarios. Scenario 2 is interesting in that it is simulating climatic conditions 50% wetter than the baseline run, yet it still generates chine forms akin to those observed on the Isle of Wight. This appears to be due to the increased rate of SLR and associated cliff retreat at operation within this scenario compensating for the enhanced knickpoint migration rate induced by the wetter climate, preserving realistic (i.e. relatively small) Chine extents overall.

Taken together, our simulations seem to suggest that it is the rate of SLR that is the key control on contemporary Chine morphology. Specifically, for this region rates of SLR, and resulting CRRs, remain high throughout much of the Holocene, only bottoming out at about 2000 cal. years BP. Prior to this time, none of the simulation scenarios have rates of knickpoint recession that are sufficiently high to match the rate of cliff retreat. This is despite the fact that catchment drainage areas, effective precipitation and the corresponding rates of knickpoint recession are all at their highest values early in the simulations. The net result is that knickpoint recession in the early to mid-Holocene, though rapid, merely results in the formation of small coastal gullies or waterfall type features of the type depicted in Figure 9(b). These features are not only small

DOI: 10.1002/esp

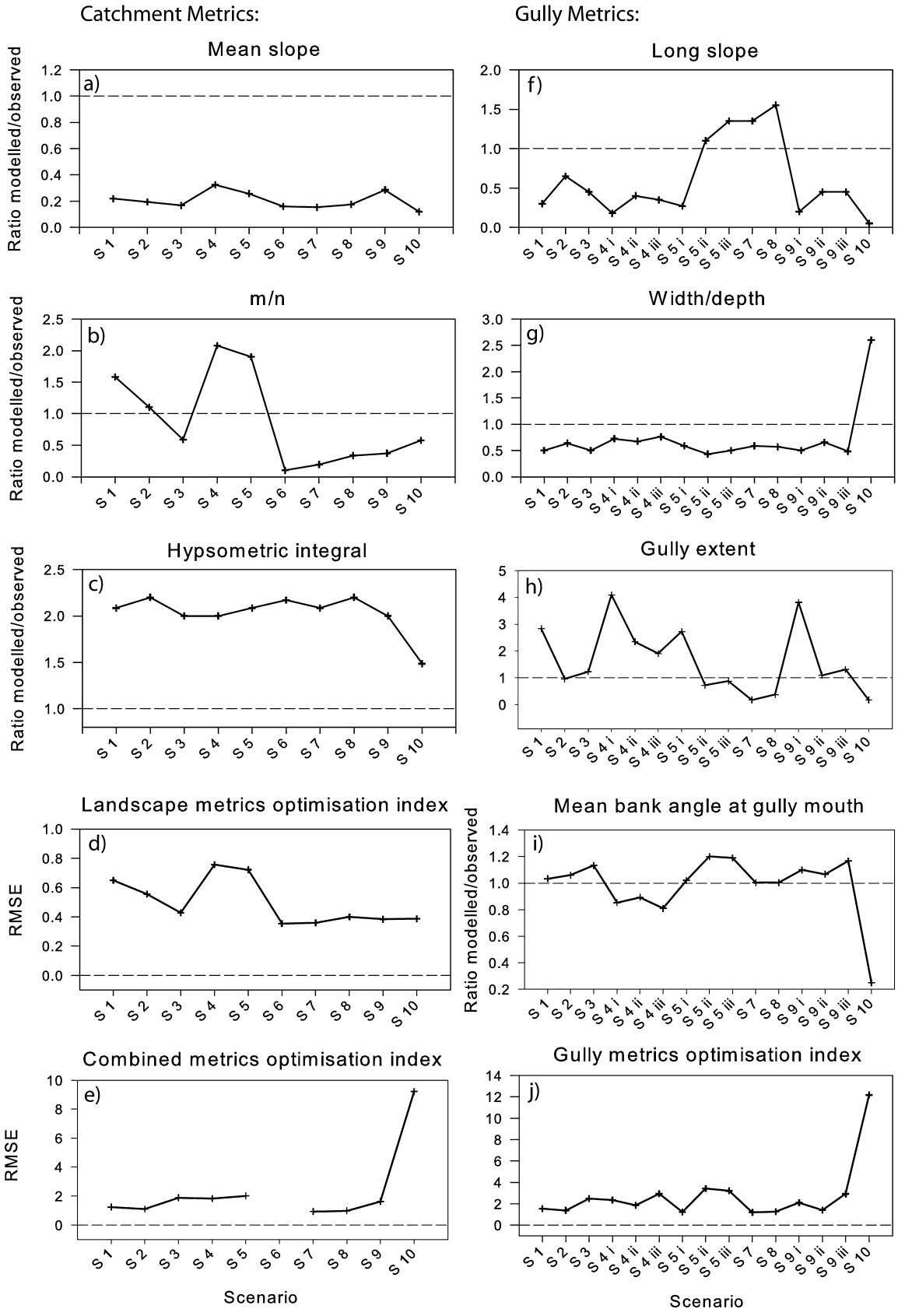

Figure 10. Ratios of modelled to observed metrics for the catchments (mean slope, *m*/*n*, hypsometric integral) and the gullies (long slope, width/depth, bank angle at mouth, extent) for each model scenario. For the gully metrics, secondary gullies from model outputs are also included where they formed (Scenarios 4, 5 and 9 – see Figure 9). Reference lines show the perfect fit between modelled and observed metrics. The optimization indices are calculated by summing the root mean squared error (RMSE) of (d) the landscape metrics, (j) the gully metrics, and (e) all metrics.

DOI: 10.1002/esp

Table III. Modelled and observed catchment and gully metrics

	Catchment metrics					Gully metrics					
Scenario	Mean slope (m m^{-1})	k_s	θ (m/n)	R^2	Normalized hypsometric integral	Long slope (m m^{-1})	Slope ratio	W/D ratio	Elevation of gully mouth (m)	Mean bank angle at mouth (deg)	Gully extent (km^2)
1	0·02	4·6	0·65	0·95	0·73	0·06	3·9	2·9	10	31	0·1
2	0·01	1·7	0·45	0·75	0·77	0·13	9·6	3·7	24	32	0·035
3	0·01	0·9	0·24	0·57	0·70	0·09	7·7	2·9	8	34	0·045
4 Gully i	0·02	13·5	0·85	0·91	0·70	0·04	1·6	4·2	7	26	0·15
Gully ii						0·08	3·5	3·9	7	27	0·086
Gully iii						0·07	3·1	4·4	8	24	0·07
5 Gully i	0·02	8·5	0·78	0·92	0·73	0·05	3·0	3·4	7	31	0·1
Gully ii						0·22	12·2	2·5	34	36	0·027
Gully iii						0·27	15·0	2·9	23	36	0·032
6	0·01	0·3	0·04	0·27	0·76	n/a	n/a	n/a	n/a	n/a	n/a
7	0·01	0·4	0·08	0·86	0·73	0·27	25·2	3·4	25	30	0·0063
8	0·01	0·5	0·14	0·67	0·77	0·31	25·4	3·3	49	30	0·014
9 Gully i	0·02	0·6	0·15	0·74	0·70	0·04	2·0	2·9	7	33	0·14
Gully ii						0·09	4·5	3·8	8	32	0·04
Gully iii						0·09	4·5	2·8	7	35	0·048
10	0·01	0·7	0·24	0·98	0·52	0·01	1·2	15·1	0·7	8	0·0063
Observed mean	0·07	0·1	0·41		0·35	0·2	3	5·8	8	30	0·037
± 1 standard deviation	± 0·04	± 0·04	± 0·04		± 0·06	± 0·04	± 0·9	± 1·4	± 10	± 4	± 0·042

Note: Where secondary gullies have formed in the area of interest they are highlighted (see Figure 9) and are analysed independently here. k_s and θ are found from regression analysis of area-slope data (R^2 indicating the goodness-of-fit of the regression). The slope ratio is the ratio of gully slopes to mean catchment slopes for the modelled and observed features.

in extent, they are also ephemeral in the sense that they are continually erased by coastal recession before reforming. It is not until the rate of SLR cliff retreat slows sufficiently that there is an opportunity for a process 'cross-over' to occur. In this case rates of knickpoint migration finally exceed rates of cliff recession, such that the Chines grow in extent and become 'permanent' features. In the case of the plausible simulation scenarios (Scenarios 2, 7 and 8) this rate of growth (i.e. the degree to which knickpoint migration rates exceed CRRs) is sufficiently small that, even after approximately 2000 years of evolution, the Chine networks remain realistically small in extent. In contrast, implausible scenarios either have rates of knickpoint migration that are too high (resulting in overly extensive gully networks; Scenarios 1, 4, 5 and 9) or too low (such that no network forms at all; Scenarios 6 and 10). It is worth noting that the bifurcation that is present in many of the simulations (see Figure 8) is observed in the Isle of Wight Chines where knickpoint recession captures an existing tributary stream.

Conclusion

The Chines of the Isle of Wight are a specific type of gully that exhibit interesting morphologies under the control of a counter-intuitive driver of development in cliff retreat, which whilst truncating the features also creates knickpoints which migrate upstream. Unsurprisingly, little is known about the long-term history of these gullies and this study has attempted to provide some context for their Holocene (12 000 years) evolution. The GOLEM (Tucker and Slingerland, 1994, 1996, 1997) was modified to include simple representation of coastal erosion processes, and following parameterization was employed with the aim of elucidating the erosional histories of the Chines.

Our model results go some way to revealing the secrets behind the long-term evolution of the Chines on the Isle of Wight. Specifically they point to the likelihood that the Chines have formed in the late Holocene. This initially appears counter-intuitive in that this period is a time of relatively low effective precipitation, but the key control on Chine evolution is the rate of SLR. Specifically, it is only in the last 2000 years that SLR has slowed sufficiently for knickpoint recession rates to exceed CRRs and create sustainable gully networks. It is noteworthy that the conclusion that the Isle of Wight gullies are of modern origin is in agreement with previous interpretations (Flint, 1982; May and Hansom, 2003).

Our results also offer some other intriguing implications. First, it is clear that more extensive Chine networks might have formed under the much wetter conditions encountered in the early Holocene had they not been erased by rapid shoreline encroachment induced by the rapid rate of SLR in this period. This implies that cliffed coasts with similar climate histories but very different sea-level responses (e.g. falling sea-level or relatively slower SLR) may characteristically have much more extensive gully networks. Therefore, the results of this study are extendable to coastal environments beyond the Isle of Wight, where sea-level and environmental histories may manifest themselves through very different gully morphologies. Second, we note that the plausible simulation scenarios in our study correspond to cases in which the rate of knickpoint migration exceeds the predicted CRR by amounts that are small enough that, even after approximately 2000 years of evolution, the simulated gully networks remain relatively small in extent. The point at which the Chine gully systems appear to be close to the critical cross-over state suggests that future gully evolution is likely to be highly sensitive to small changes in future rates of effective precipitation and/or SLR. Finally, the fact that our plausible model scenarios do appear to exist close to a key process threshold merely reinforces the need to consider the intrinsic limitations of the study. Specifically, in related research we are currently investigating the degree to which uncertainties in the values of key model parameters (not considered here, but which from sensitivity analysis have been identified as k_b, Φ_c and S_{cr} from Equations A6 and A8 in the Appendix) may influence the degree to which our preliminary conclusions can be considered robust.

DOI: 10.1002/esp

Acknowledgements—JL gratefully acknowledges PhD funding from the England and Wales Environment Agency and the School of Geography, University of Southampton.

References

Ambers RKR, Druckenbrod DL, Ambers CP. 2006. Geomorphic response to historical agriculture at Monument Hill in the Blue Ridge foothills of central Virginia. *Catena* **65**(1): 49–60. DOI. 10.1016/j.catena.2005.09.002.

Anderson DE, Binney HA, Smith MA. 1998. Evidence for abrupt climatic change in northern Scotland between 3900 and 3500 calendar years BP. *The Holocene* **8**(1): 97–103.

Arnell NW. 2003. Effects of IPCCSRES emissions scenarios on river runoff: a global perspective. *Hydrology and Earth System Sciences* **7**(5): 619–641.

Barber KE. 1987. *Wessex and the Isle of Wight – Field Guide*. Quaternary Research Association: Cambridge.

Barber KE, Langdon P. 2001. Testing the palaeoclimatic signal from peat bogs – temperature or precipitation forcing? Paper presented at the *PAGES-PEPIII/ESF-HOLIVAR International Conference: Past Climate Variability Through Europe and Africa*, France.

Bird E. 1997. *The Shaping of the Isle of Wight*. Cromwell Press: Trowbridge.

Bishop P. 2007. Long-term landscape evolution: linking tectonics and surface processes. *Earth Surface Processes and Landforms* **32**(3): 329–365.

Bishop P, Hoey TB, Jansen JD, Artza IL. 2005. Knickpoint recession rate and catchment area: The case of uplifted rivers in Eastern Scotland. *Earth Surface Processes and Landforms* **30**: 767–778. DOI. 10.1002/esp.1191.

Boardman J, Poesen J (eds). 2006. *Soil Erosion in Europe*. John Wiley & Sons: Chichester.

Bray MJ, Carter DJ, Hooke JM. 2004. *Quaternary History of the Solent System. Coastal Sediment Transport Study – Report to Coastal Groups*. University of Portsmouth: Portsmouth.

Bray MJ, Hooke JM. 1997. Prediction of soft-cliff retreat with accelerating sea-level rise. *Journal of Coastal Research* **13**(2): 453–467.

Burkard MB, Kostaschuk RA. 1995. Initiation and evolution of gullies along the shoreline of Lake Huron. *Geomorphology* **14**: 211–219. DOI. 10.1016/0169-555X(95)00059-E.

Chiverrell RC, Harvey AM, Foster GC. 2007. Hillslope gullying in the Solway Firth – Morecambe Bay region, Great Britain: responses to human impact and/or climatic deterioration? *Geomorphology* **84**: 317–343. DOI. 10.1016/j.geomorph.2005.12.014|ISSN 0169-555X.

Clark PU, Mix AC. 2002. Ice sheets and sea level of the Last Glacial Maximum. *Quaternary Science Reviews* **21**: 1–7. DOI. 10.1016/S0277-3791(01)00118-4.

Coulthard T. 1999. *Modelling Upland Catchment Response to Holocene Environmental Change*. University of Leeds: Leeds.

Coulthard T, Kirkby MJ, Macklin MG. 2000. Modelling geomorphic response to environmental change in an upland catchment. *Hydrological Processes* **14**: 2031–2045.

Coulthard T, Macklin MG, Kirkby MJ. 2002. A cellular model of holocene upland river basin and alluvial fan evolution. *Earth Surface Processes and Landforms* **27**: 269–288.

Crosby BT, Whipple KX. 2006. Knickpoint initiation and distribution within fluvial networks: 236 waterfalls in the Waipaoa River, North Island, New Zealand. *Geomorphology* **82**(1–2): 16–38.

Daley B, Insole A. 1984. *The Isle of Wight*. The Geologist's Association: London.

Davis BAS, Brewer S, Stevenson AC, Guiot J. 2003. The temperature of Europe during the Holocene reconstructed from pollen data. *Quaternary Science Reviews* **22**(15–17): 1701–1716.

Dyer KR. 1975. The buried channels of the 'Solent River', southern England. *Proceedings of Geologists' Association* **86**: 239–245.

Edwards RJ. 2001. Mid- to late Holocene relative sea-level change in Poole Harbour, southern England. *Journal of Quaternary Science* **16**(3): 221–235. DOI. 10.1002/jqs.585.

Emery KO, Kuhn GG. 1982. Sea cliffs – their processes, profiles, and classification. *Geological Society of America Bulletin* **93**(7): 644–654. DOI. 10.1130/0016-7606(1982)93⟨644:SCTPPA⟩2.0.CO;2.

Everard CE. 1954. The Solent River: a geomorphological study. *Transactions and Papers (Institute of British Geographers)* **20**: 41–58.

Flint KE. 1982. Chines on the Isle of Wight: channel adjustment and basin morphology in relation to cliff retreat. *The Geographical Journal* **148**(2): 225–236.

Greig SM, Sear DA, Carling PA. 2005. The impact of fine sediment accumulation on the survival of incubating salmon progreny: implications for sediment management. *Science of the Total Environment* **344**(1–3): 241–258. DOI. 10.1016/j.scitotenv.2005.02.010.

Hampton MA, Griggs GB (eds). 2004. *Formation, Evolution and Stability of Coastal Cliffs – Status and Trends*, USGS Professional Paper 1693. US Geological Survey: Reston, VA.

Howard AD. 1997. Badland morphology and evolution: interpretation using a simulation model. *Earth Surface Processes and Landforms* **22**: 211–227.

Howard AD. 1999. Simulation of gully erosion and bistable landforms. In *Incised River Channels: Processes, Forms, Engineering and Management* John Wiley & Sons: Chichester; 277–300.

Istanbulluoglu E, Bras RL, Flores-Cervantes H, Tucker GE. 2005. Implications of bank failures and fluvial erosion for gully development: field observations and modeling. *Journal of Geophysical Research – Earth Surface* **110**(F1): F01014.

Knighton D. 1998. *Fluvial Forms and Processes: A New Perspective*. Arnold: London.

Kohn BP, Gleadow AJW, Brown RW, Gallagher K, O'Sullivan PB, Foster DA. 2002. Shaping the Australian crust over the last 300 million years: insights from fission track thermotectonic imaging and denudation studies of key terranes. *Australian Journal of Earth Sciences* **49**(4): 697–717. DOI. 10.1046/j.1440-0952.2002.00942.x.

Lambeck K. 1991. Glacial rebound and sea-level change in the British Isles. *Terra Nova* **3**: 379–389. DOI. 10.1111/j.1365-3121.1991.tb00166.x.

Lee EM. 1997. The investigation and management of soft rock cliffs. Paper presented at the *Proceedings of MAFF Conference of River and Coastal Engineers*. July 1997, Keele, UK.

Lee EM, Clark AR. 2002. *Prediction of Recession Rates and Erosion Control Techniques. DEFRA Flood Management Division – R and D Report.* DEFRA: London.

Leopold LB, Wolman MG, Miller JP. 1964. *Fluvial Processes in Geomorphology*. W. H. Freeman: San Francisco, CA.

Leyland J, Darby SE. 2008. An empirical-conceptual gully evolution model for channelled sea cliffs. *Geomorphology* **102**: 419–434. DOI. 10.1016/j.geomorph.2008.04.017.

Long AJ, Scaife RG, Edwards RJ. 1999. Pine pollen in intertidal sediments from Poole Harbour, UK; implications for late-Holocene sediment accretion rates and sea-level rise. *Quaternary International* **55**: 3–16. DOI. 10.1016/S1040-6182(98)00017-2.

Long AJ, Scaife RG, Edwards RG. 2000. Stratigraphic architecture, relative sea level, and models of estuary development in southern England: new data from Southampton Water. In *Coastal and Estuarine Environments: Sedimentology, Geomorphology and Geoarchaeology*, Pye K, Allen JRL (eds). Geological Society: London; 253–279.

Long AJ, Tooley MJ. 1995. Holocene sea-level and crustal movements in Hampshire and southeast England, United Kingdom. *Journal of Coastal Research* **17**: 299–310.

Mathworks. 2008. *The MathWorks – MATLAB and Simulink for Technical Computing.* http://www.mathworks.com [21 November 2008].

May VJ, Hansom JD. 2003. *Coastal Geomorphology of Great Britain*. Joint Nature Conservation Committee: Peterborough.

Mottershead DN. 1997. A morphological study of Greenschist weathering on dated coastal structures, South Devon, UK. *Earth Surface Processes and Landforms* **22**(5): 491–506.

Nachtergaele J, Poesen J, Steegen A, Takken I, Beuselinck L, Vandekerckhove L, Govers G. 2001. The value of a physically based model versus an empirical approach in the prediction of ephemeral gully erosion for loess-derived soils. *Geomorphology* **40**(3–4): 237–252.

New M, Hulme M, Jones P. 1999. Representing twentieth-century space-time climate variability. Part I: Development of a 1961–90

mean monthly terrestrial climatology. *Journal of Climate* **12**(3): 829–856.
Nicholls RJ. 1987. Evolution of the upper reaches of the Solent River and the formation of Poole and Christchurch bays. In *Wessex and the Isle of Wight – Field Guide*, Barber KE (ed.). Quaternary Research Association: Cambridge; 99–114.
Nowell DAG. 2000. Discussion on late Quaternary evolution of the upper reaches of the Solent River, southern England, based upon marine geophysical evidence. *Journal of the Geological Society* **157**: 505–507.
Poesen J, Nachtergaele J, Verstraeten G, Valentin C. 2003. Gully erosion and environmental change: importance and research needs. *Catena* **50**(2–4): 91–133. DOI. 10.1016/S0341-8162(02)00143-1.
Rosenbloom NA, Anderson RS. 1994. Hillslope and channel evolution in a marine terraced landscape, Santa-Cruz, California. *Journal of Geophysical Research – Solid Earth* **99**(B7): 14013–14029.
Schumm SA, Harvey MD, Watson CC. 1984. *Incised Channels: Morphology, Dynamics and Control*. Water Resources Publications: Chelsea, MI.
Schumm SA, Phillips L. 1986. Composite channels of the Canterbury Plain, New Zealand – a Martian analog. *Geology* **14**(4): 326–329.
Shennan I, Horton B. 2002. Holocene land- and sea-level changes in Great Britain. *Journal of Quaternary Science* **17**(5–6): 511–526. DOI. 10.1002/jqs.710.
Simon A, Rinaldi M, Hadish G. 1996. Channel evolution in the loess area of the midwestern United States. Paper presented at the *Proceedings of the Sixth Federal Interagency Sedimentation Conference*. March 1996, Las Vegas, US.
Stankoviansky M. 2003. Historical evolution of permanent gullies in the Myjava Hill Land, Slovakia. *Catena* **51**(3–4): 223–239.
Stock JD, Montgomery DR. 1999. Geologic constraints on bedrock river-incision using the stream power law. *Journal of Geophysical Research* **104**: 4983–4993.
Summerfield MA. 1991. *Global Geomorphology*. Pearson Education: Harlow.
Suren AM, Martin ML, Smith BJ. 2005. Short-term effects of high suspended sediments on six common New Zealand stream invertebrates. *Hydrobiologia* **548**: 67–74. DOI. 10.1007/s10750-005-4167-5.
Tolhurst TJ, Black KS, Shayler SA, Mather S, Black I, Baker K, Paterson DM. 1999. Measuring the in situ erosion shear stress of intertidal sediments with the Cohesive Strength Meter (CSM). *Estuarine Coastal and Shelf Science* **49**(2): 281–294.
Tubbs C. 1999. *The Ecology, Conservation and History of the Solent*. Packard Publishing Limited: Chichester.
Tucker GE, Bras RL. 1998. Hillslope processes, drainage density, and landscape morphology. *Water Resources Research* **34**(10): 2751–2764.
Tucker GE, Slingerland R. 1994. Erosional dynamics, flexural isostasy, and long-lived escarpments: a numerical modeling study. *Journal of Geophysical Research – Solid Earth* **99**(B6): 12229–12243. DOI. 10.1029/94JB00320.
Tucker GE, Slingerland R. 1996. Predicting sediment flux from fold and thrust belts. *Basin Research* **8**(3): 329–349. DOI. 10.1046/j.1365-2117.1996.00238.
Tucker GE, Slingerland R. 1997. Drainage basin responses to climate change. *Water Resources Research* **33**(8): 2031–2047. DOI. 10.1029/97WR00409.
Tucker GE, Whipple KX. 2002. Topographic outcomes predicted by stream erosion models: sensitivity analysis and intermodel comparison. *Journal of Geophysical Research – Solid Earth* **107**(B9): 2179.
Valentin C, Poesen J, Li Y. 2005. Gully erosion: impacts, factors and control. *Catena* **63**(2–3): 132–153. DOI. 10.1016/j.catena.2005.06.001|ISSN 0341-8162.
Vandekerckhove L, Poesen J, Wijdenes DO, Nachtergaele J, Kosmas C, Roxo MJ, de Figueiredo T. 2000. Thresholds for gully initiation and sedimentation in Mediterranean Europe. *Earth Surface Processes and Landforms* **25**(11): 1201–1220.
Vanwalleghem T, Poesen J, Van Den Eeckhaut M, Nachtergaele J, Deckers J. 2005. Reconstructing rainfall and land-use conditions leading to the development of old gullies. *Holocene* **15**(3): 378–386. DOI. 10.1191/0959683605hl807rp.
Vanwalleghem T, Van Den Eeckhaut M, Poesen J, Deckers J, Nachtergaele J, Van Oost K, Slenters C. 2003. Characteristics and controlling factors of old gullies under forest in a temperate humid climate: a case study from the Meerdaal Forest (Central Belgium). *Geomorphology* **56**(1–2): 15–29.
Velegrakis AF, Dix JK, Collins MB. 1999. Late Quaternary evolution of the upper reaches of the Solent River, Southern England, based upon marine geophysical evidence. *Journal of the Geological Society* **156**: 73–87. DOI. 10.1144/gsjgs.156.1.0073.
Velegrakis AF, Dix JK, Collins MB. 2000. Late Pleistocene/Holocene evolution of the upstream section of the Solent River. In *Solent Science – A Review*, Collins MB, Ansell K (eds). Elsevier Science: Amsterdam; 97–99.
von Blanckenburg F, Hewawasam T, Kubik PW. 2004. Cosmogenic nuclide evidence for low weathering and denudation in the wet, tropical highlands of Sri Lanka. *Journal of Geophysical Research – Earth Surface* **109**(F3). DOI. F03008 Artn f03008.
Walkden M, Dickson M. 2006. *The Response of Soft Rock Shore Profiles to Increased Sea-level Rise*. Tyndall Centre for Climate Change Research: Norwich.
Waller MP, Long AJ. 2003. Holocene coastal evolution and sea-level change on the southern coast of England: a review. *Journal of Quaternary Science* **18**(3–4): 351–359. DOI. 10.1002/jqs.754.
West IM. 1980. Geology of the Solent Estuarine System. In *The Solent Estuarine System: An Assessment of Present Knowledge (NERC Publication Series C, No. 22)*. Natural Environment Research Council: London; 6–18.
Whipple KX, Hancock GS, Anderson RS. 2000. River incision into bedrock: mechanics and relative efficacy of plucking, abrasion, and cavitation. *Geological Society of America Bulletin* **112**(3): 490–503.
Whipple KX, Tucker GE. 2002. Implications of sediment-flux-dependent river incision models for landscape evolution. *Journal of Geophysical Research* **107**(B2): 2039.
Wobus CW, Whipple K, Kirby E, Snyder N, Johnson J, Spyropolou K, Crosby BT, Sheehan D. 2006. Tectonics form topography: procedure, promise, and pitfalls. In *Tectonics, Climate, and Landscape Evolution*, Willett SD, Hovius N, Brandon MT, Fisher DM (eds), Geological Society of America Special Paper 398, Penrose Conference Series. Geological Society of America: Boulder, CO; 55–74.

Appendix

Description of GOLEM

The mass continuity and process equations introduced below, along with Figure 3, are all taken from Tucker and Slingerland (1997). GOLEM includes the state variables of surface elevation (h), bedrock elevation (R) and regolith thickness (C) all measured in metres. The mass continuity equation for surface elevation, h, at a given time is found by:

$$h = R + C \tag{A1}$$

The continuity of bedrock mass is described as:

$$\frac{\delta R}{\delta t} = U - \omega - E \tag{A2}$$

where U is the uplift rate (in m a^{-1}), ω is the weathering rate (in m a^{-1}) and E is the bedrock channel erosion rate (in m a^{-1}). Finally, the continuity of regolith mass is given as:

$$\frac{\delta C}{\delta t} = \omega - \nabla Q_s - \nabla q_m \tag{A3}$$

where Q_s is the volumetric overland or channelized sediment transport rate per unit channel width (in $m^3\ a^{-1}$) and q_m is the volumetric hillslope mass movement transport rate per unit slope width (in $m^3\ a^{-1}$).

The rate of weathering, ω, in continuity Equation A2 is given by:

$$\omega = k_w \exp^{-C/m_w} \tag{A4}$$

where k_w is the weathering rate coefficient (in $m\ a^{-1}$) for bare bedrock, C is the regolith thickness and m_w is a parameter that governs the rate at which bedrock to sediment conversion decays with increasing regolith thickness (in metres). Weathering only occurs in cells where the drainage area, A (in m^2), falls below a critical threshold for permanent (non-weathering) channels, A_{cr} (in m^2). Diffusive (slope driven) mass movement processes, such as soil creep, are represented using:

$$q_m = -k_d \nabla h \tag{A5}$$

where k_d is the diffusivity coefficient (in $m^2\ a^{-1}$). Mass wasting, both of regolith and bedrock, occurs when:

$$S > S_{cr} \tag{A6}$$

where S is the local slope gradient (in $m\ m^{-1}$) and S_{cr} is the threshold gradient for landsliding (in $m\ m^{-1}$). The default fluvial erosion function in GOLEM is a simple power law relationship of the form:

$$Q_s = k_f Q^{m_f} S^{n_f} \tag{A7}$$

where Q_s is the volumetric rate of sediment transport per unit width, k_f is a dimensionless sediment transport efficiency coefficient, Q is the flow discharge per unit width (in $m^3\ s^{-1}$), S is the channel slope and m and n are dimensionless exponents on the discharge and slope terms, respectively. Bedrock erosion only occurs in GOLEM once a cell has been stripped of regolith cover, and is calculated thus:

$$E = k_b(Q^{m_b} S^{n_b} - \Phi_c) \tag{A8}$$

where k_b is the bedrock erodibility coefficient (which has dimensions, $L^{(1-2\ m)}\ T^{-1}$, that depend on the value of m), m_b and n_b are the dimensionless bedrock area and slope exponents, respectively and Φ_c is a bedrock erosion shear stress threshold term (in $m\ a^{-1}$).

DOI: 10.1002/esp